

# ChemComm

Chemical Communications

Accepted Manuscript

This article can be cited before page numbers have been issued, to do this please use: Y. Wang, H. Huang, S. Zhang, H. Zhang, L. Zhang, C. Jing and J. Wang, *Chem. Commun.*, 2024, DOI: 10.1039/D4CC03845B.



This is an Accepted Manuscript, which has been through the Royal Society of Chemistry peer review process and has been accepted for publication.

Accepted Manuscripts are published online shortly after acceptance, before technical editing, formatting and proof reading. Using this free service, authors can make their results available to the community, in citable form, before we publish the edited article. We will replace this Accepted Manuscript with the edited and formatted Advance Article as soon as it is available.

You can find more information about Accepted Manuscripts in the [Information for Authors](#).

Please note that technical editing may introduce minor changes to the text and/or graphics, which may alter content. The journal's standard [Terms & Conditions](#) and the [Ethical guidelines](#) still apply. In no event shall the Royal Society of Chemistry be held responsible for any errors or omissions in this Accepted Manuscript or any consequences arising from the use of any information it contains.

## COMMUNICATION

Hydroxylation boosted low-overpotential CO<sub>2</sub> reduction to ethylene for Cu/PTFE electrodeYifeng Wang<sup>a,b</sup>, Haoliang Huang<sup>a</sup>, Shengjie Zhang<sup>a</sup>, Hao Zhang<sup>a</sup>, Chao Jing<sup>\*a,b</sup>, Jian-Qiang Wang<sup>\*a,b</sup>, Linjuan Zhang<sup>\*a,b</sup>Received 00th January 20xx,  
Accepted 00th January 20xx

DOI: 10.1039/x0xx00000x

**We present a Cu/PTFE electrode for CO<sub>2</sub> reduction reaction with high coverage of \*OH which facilitates both the activation of CO<sub>2</sub> and the C-C coupling, leading to a Faradaic efficiency for ethylene exceeding 50% at an exceptionally low potential of -246 mV vs. RHE, with a maximum FE<sub>C<sub>2</sub>H<sub>4</sub></sub> reaching 60.3%.**

The escalating global levels of CO<sub>2</sub> and the excessive consumption of fossil fuels present major obstacles to sustainable development.<sup>1-3</sup> The CO<sub>2</sub> reduction reaction (CO<sub>2</sub>RR), powered by renewable energy, emerges as a viable solution for CO<sub>2</sub> conversion while generating high-value chemicals under ambient conditions. Among various products of the electrochemical CO<sub>2</sub>RR, multi-carbon compounds especially ethylene have garnered significant attention due to their versatility in industry.<sup>4-6</sup> Cu is the only single-metal catalyst capable of reducing CO<sub>2</sub> into diverse multi-carbon compounds, owing to the appropriate adsorption energy for \*CO and \*H species.<sup>7,8</sup> Cu-based catalysts are thus extensively employed in CO<sub>2</sub>RR to produce ethylene, however, there are still challenges including high overpotentials,<sup>9,10</sup> limited ethylene selectivity,<sup>11,12</sup> and competing hydrogen evolution reactions.<sup>13,14</sup>

Among Cu-based catalysts, Cu(OH)<sub>2</sub> exhibits notable selectivity towards the production of ethylene in CO<sub>2</sub>RR, attributed to the high \*OH coverage on the Cu surface derived from Cu(OH)<sub>2</sub> during the CO<sub>2</sub>RR process.<sup>15,16</sup> The presence of \*OH promotes the adsorption of CO at an atop site (\*CO<sub>atop</sub>) on Cu rather than at a bridge site (\*CO<sub>bridge</sub>)<sup>17</sup> and impacts the work function of the Cu surface,<sup>18</sup> which promotes the C-C coupling to generate C<sub>2+</sub> products. Many efforts have been contributed to further enhance the ethylene selectivity of Cu(OH)<sub>2</sub> catalysts, including morphology and facet engineering,<sup>19,20</sup> tuning surface \*OH amounts and particle size<sup>15,18</sup> and microenvironment control.<sup>21</sup> Polytetrafluoroethylene (PTFE) has been used to suppress the hydrogen evolution side reaction by enhancing the local hydrophobic environment of the catalyst and augmenting

the solid-liquid-gas interfaces, which effectively enhances the selectivity for C<sub>2</sub>H<sub>4</sub>.<sup>14,21</sup> In addition to the selectivity, the overpotential for CO<sub>2</sub>RR stands as a pivotal merit for evaluating electrocatalytic performance. For most CO<sub>2</sub>RR catalysts, the overpotentials required for achieving high selectivity (over 50%) of ethylene typically exceed 500 mV.<sup>10,22,23</sup> These high overpotentials are commonly attributed to the significant energy barriers associated with the first step of CO<sub>2</sub> activation and the step of carbon-carbon coupling. Achieving both high ethylene selectivity and low overpotentials remains a significant challenge in the realm of CO<sub>2</sub>RR.

In this study, to enhance the active sites and catalytic ability, an ion sputtering method was employed to deposit nano-sized Cu catalysts onto the PTFE membrane, to obtain uniformly dispersed Cu/PTFE electrode with good hydrophobicity and sufficient mechanical strength (Fig. S1 and S2). Furthermore, to modulate the surface \*OH, Cu particles were sputtered under dry and moist Ar atmospheres, denoted as D\_Cu and M\_Cu, respectively. The moist atmosphere was achieved by introducing water molecules through the addition of a hygroscopic polylactide (PLA) material into the vacuum chamber of the ion sputtering coater, which facilitated the formation of Cu(OH)<sub>2</sub> (Fig. 1a and Fig. S3, ESI<sup>†</sup>). Experimental results demonstrated that our M\_Cu catalyst exhibited high selectivity and low overpotential for the generation of ethylene, with a Faradaic efficiency for ethylene (FE<sub>C<sub>2</sub>H<sub>4</sub></sub>) of 55.1% at a low potential of -246 mV vs. reversible hydrogen electrode (RHE), and the highest FE<sub>C<sub>2</sub>H<sub>4</sub></sub> reached 60.3%. This superior electrochemical performance was attributed to the abundant coverage of \*OH on the surface of the nano-sized Cu catalyst. Density Functional Theory (DFT) simulations elucidated that the presence of \*OH on the Cu catalyst surface lowers both the barriers of CO<sub>2</sub> activation and C-C coupling, thereby efficiently decreasing the overpotential and enhancing the selectivity for ethylene.

The morphology of the as-prepared Cu-sputtered PTFE electrodes was characterized using field-emission scanning electron microscopy (FESEM). The ion-sputtered Cu species were coated uniformly on PTFE fibers while maintaining the porous structure, which facilitated the gas diffusion of CO<sub>2</sub> from the back to the Cu front (Fig. 1c and Fig. S4-5, ESI<sup>†</sup>). The

<sup>a</sup> Key Laboratory of Interfacial Physics and Technology, Shanghai Institute of Applied Physics, Chinese Academy of Sciences, Shanghai 201800, P. R. China.

<sup>b</sup> University of Chinese Academy of Sciences, Beijing 100049, P. R. China.

<sup>c</sup> Songshan Lake Materials Laboratory, Dongguan 523808, P. R. China.

<sup>†</sup> Electronic supplementary Information (ESI) available. See DOI: 10.1039/x0xx00000x



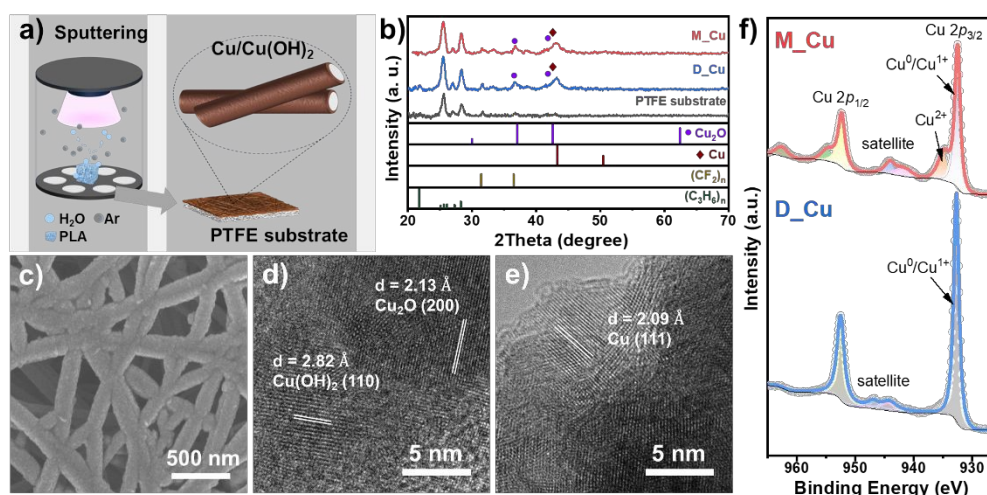


**Fig. 1** (a) Schematic illustration of the method for the deposition of Cu/Cu(OH)<sub>2</sub> catalysts onto polytetrafluoroethylene (PTFE) substrate via ion sputtering in moist Ar atmosphere. (b) Grazing incidence X-ray diffraction (GI-XRD) patterns of M\_Cu, D\_Cu and PTFE substrate (with (CF<sub>2</sub>)<sub>n</sub> (JCPDS#54-1594), (C<sub>3</sub>H<sub>6</sub>)<sub>n</sub> (JCPDS#54-1936), Cu<sub>2</sub>O (JCPDS#34-1354) and Cu (JCPDS #04-0836) as references). (c) Field-emission scanning electron microscopy (FESEM) of M\_Cu. (d), (e) High-resolution transmission electron microscopy (HRTEM) of M\_Cu. (f) X-ray photoelectron spectroscopy (XPS) of M\_Cu and D\_Cu.

crystalline phase of the Cu catalysts was identified using grazing incidence X-ray diffraction (GI-XRD) (Fig. 1b). Apart from the characteristic peaks of (CF<sub>2</sub>)<sub>n</sub> and (C<sub>3</sub>H<sub>6</sub>)<sub>n</sub> from the polypropylene-supported PTFE membrane, M\_Cu and D\_Cu showed diffraction patterns matched with Cu<sub>2</sub>O and metallic Cu. We assume that the formation of Cu<sub>2</sub>O is due to the rapid oxidation of Cu nanoparticles upon exposure to air. From the high-resolution transmission electron microscopy (HRTEM) in Fig. S6 (ESI<sup>†</sup>), the lattice fringes of 0.208 and 0.213 nm of D\_Cu match well with the Cu (111) and Cu<sub>2</sub>O (200), indicating the coexistence of Cu and Cu<sub>2</sub>O, consistent with the XRD analysis. For M\_Cu (Fig. 1d–e), lattice fringes with interplanar spacings of 0.209, 0.213, and 0.282 nm were observed, aligning with the Cu (111), Cu<sub>2</sub>O (200), and the (110) lattice plane of Cu(OH)<sub>2</sub>, respectively. We assume that the formation of Cu(OH)<sub>2</sub> was facilitated by the introduction of H<sub>2</sub>O molecules during the sputtering process. Elemental mapping conducted to assess the distribution of Cu along individual PTFE fibers (Fig. S7, ESI<sup>†</sup>) demonstrated the co-localization of Cu, O, C, and F in both M\_Cu and D\_Cu, signifying the uniform coating of sputter-deposited Cu onto the PTFE fibers. The presence of O is attributed to the oxidation of Cu in the ambient air.

X-ray photoelectron spectroscopy (XPS) analysis was used to further investigate the chemical states of the surface Cu species (Fig. 1f). D\_Cu showed a distinct Cu 2p<sub>3/2</sub> peak at 932.6 eV and a weak satellite feature, corresponding to Cu<sup>0</sup>/Cu<sup>1+</sup>. It is difficult to distinguish the oxidation states of Cu<sup>0</sup> and Cu<sup>1+</sup> using the Cu 2p<sub>3/2</sub> peak since the binding energies of the two species are too close. For M\_Cu, apart from the sharp Cu<sup>0</sup>/Cu<sup>1+</sup> peak, a shoulder at a higher binding energy (934.7 eV) was clearly observed, which can be attributed to Cu(OH)<sub>2</sub>.<sup>15</sup> In addition, the Cu 2p<sub>3/2</sub> XPS of M\_Cu showed more pronounced satellite features at lower binding energy compared to D\_Cu, supporting the presence of Cu<sup>2+</sup> species. The Cu LMM Auger spectrum (Fig. S8, ESI<sup>†</sup>) showed the peak at 570.0 eV for D\_Cu and 570.4 eV for

M\_Cu, corresponding to Cu<sub>2</sub>O and Cu(OH)<sub>2</sub>, respectively.<sup>15</sup> The presence of Cu(OH)<sub>2</sub> on M\_Cu was also corroborated by the OH vibrational peaks in the infrared spectra (Fig. S9, ESI<sup>†</sup>).<sup>24</sup> Owing to their porous structure and the electrically conductive Cu coating, the Cu/PTFE electrodes were directly used as gas diffusion electrodes for CO<sub>2</sub>RR measurements. As shown in Fig. 2a, linear sweep voltammetry curves (LSV) of M\_Cu exhibited a larger current density and lower onset potential than those of D\_Cu, implying higher catalytic activity. In addition, M\_Cu showed lower charge transfer resistance and Tafel slope (Fig. S10, ESI<sup>†</sup>) than those of D\_Cu, indicating faster reaction kinetics. The Faradaic efficiency for each gaseous product of M\_Cu and D\_Cu at different current densities from -10 to -200 mA·cm<sup>-2</sup>, along with the corresponding potentials, are depicted in Fig. 2b and Fig. S11–12 (ESI<sup>†</sup>). The FE<sub>C<sub>2</sub>H<sub>4</sub></sub> of M\_Cu (Fig. 2b) reached up to 60.34% at a current density of -100 mA/cm<sup>2</sup> and achieved a long-term stability for 12h (Fig. S13, ESI<sup>†</sup>). In contrast, the optimal FE<sub>C<sub>2</sub>H<sub>4</sub></sub> of D\_Cu was only 48%. It is worthy to note that both M\_Cu and D\_Cu exhibited better CO<sub>2</sub>RR performance in comparison to commercial copper nanoparticles (Cu NPs, Fig. S14a, ESI<sup>†</sup>) and copper sputtered carbon paper (Fig. S14b, ESI<sup>†</sup>), demonstrating the advantage of our ion-sputtering method with smaller particle size and more solid-liquid-gas three-phase interfaces.

Furthermore, M\_Cu exhibits an exceptionally low overpotential, ca. -0.2 V, for catalyzing CO<sub>2</sub>RR-ethylene conversion, indicating the prompt activation of CO<sub>2</sub> to CO and subsequent coupling to ethylene. Notably, FE<sub>C<sub>2</sub>H<sub>4</sub></sub> of M\_Cu surpassed 50% when the potential reached -249 mV (Fig. 2b and Fig. S15, ESI<sup>†</sup>), demonstrating excellent performance in terms of overpotential and ethylene selectivity compared to recently reported advanced studies (Fig. 2d).<sup>25–34</sup> In addition, Fig. 2c compares the potential-dependent ethylene partial current density of the catalysts. M\_Cu exhibited nearly double the partial current density of D\_Cu and a steeper slope across the



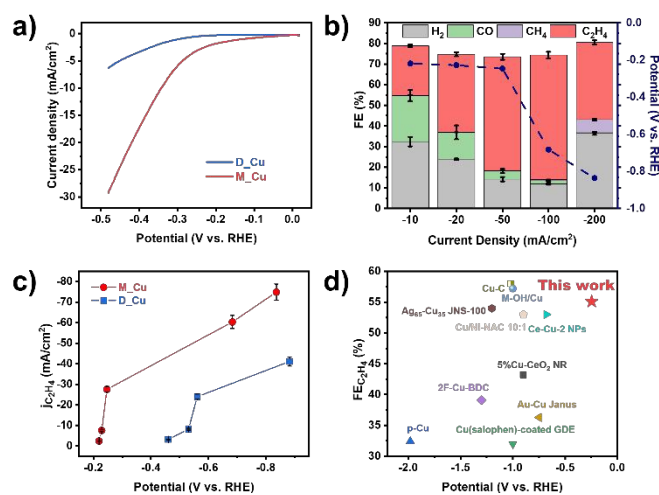


**Fig. 2** (a) Linear-sweep voltammetry curves (LSV) of M\_Cu and D\_Cu. (b) Faradaic efficiency for each CO<sub>2</sub>RR gaseous products of M\_Cu at different current densities and corresponding potentials. (c) Partial current density of C<sub>2</sub>H<sub>4</sub> of M\_Cu and D\_Cu depending on the applied potentials. (d) Comparison of Faradaic efficiency for C<sub>2</sub>H<sub>4</sub> (FE<sub>C<sub>2</sub>H<sub>4</sub></sub>) and corresponding potentials with documented CO<sub>2</sub>RR electrocatalysts.

tested potential range. These findings suggest the key function of Cu-OH species in activating CO<sub>2</sub>RR-to-ethylene at lower potentials.

In order to identify the reaction intermediates on the surface of Cu catalysts during the CO<sub>2</sub>RR, in situ Raman spectroscopy was carried out under applied potentials from open circuit potential (OCP) to -0.4 V. M\_Cu and D\_Cu were prepared on Au electrodes instead of PTFE membranes to enhance the Raman signals. The Raman spectrum of M\_Cu (Fig. 3a) showed distinct peaks at Raman shifts of 1610, 1976, and 2075 cm<sup>-1</sup> upon reaching 0.2 V. These peaks are assigned to \*CHO, \*CO<sub>bridge</sub>, and \*CO<sub>atop</sub>, respectively. The intensity of these peaks gradually reduced as the applied potential decreased from 0.1 V to -0.1 V, and diminished at -0.2 V, suggesting a faster CO<sub>2</sub>RR process at lower potentials, where the intermediate products were rapidly consumed. The peak intensity of \*CO<sub>atop</sub> is much higher than that of \*CO<sub>bridge</sub>, indicating preferential adsorption of CO at the atop site of Cu for M\_Cu, which is beneficial for carbon-carbon coupling.<sup>17</sup> In addition, two weak peaks were observed at 1060 and 1355 cm<sup>-1</sup>, corresponding to \*CO<sub>3</sub><sup>2-</sup> and \*HCO<sub>3</sub><sup>-</sup> species from the electrolyte, respectively. The in situ Raman spectra of D\_Cu (Fig. 3b) showed three peaks at 1080, 1545, 1960, and 2070 cm<sup>-1</sup> at 0 V, attributed respectively to \*CO<sub>3</sub><sup>2-</sup>, \*CHO, \*CO<sub>bridge</sub> and \*CO<sub>atop</sub> species. Comparing the Raman spectra of M\_Cu and D\_Cu, it is evident that M\_Cu exhibited significant intermediate product peaks at a lower potential (0.2 V). This observation correlates with the electrochemical results that M\_Cu displayed a lower onset potential during the CO<sub>2</sub>RR (Fig. 2b). Additionally, M\_Cu exhibited much higher peak intensity for the intermediate products compared to D\_Cu (Fig. S16, ESI<sup>†</sup>), implying higher reaction activity. Control experiments conducted on bare Au electrodes did not show observable Raman signals (Fig. S17, ESI<sup>†</sup>).

After the CO<sub>2</sub>RR experiments, M\_Cu and D\_Cu were characterized using SEM. The morphology of post-reaction D\_Cu was similar to its pristine structure (Fig. S18a, ESI<sup>†</sup>).

Surprisingly, the post-reaction M\_Cu (Fig. S18b, ESI<sup>†</sup>) showed needle-like structures, suggesting substantial restructuring of the Cu catalyst during the reaction induced by Cu-OH. In Fig. S19a (ESI<sup>†</sup>), XPS of the post-reaction M\_Cu exhibited a decrease in the area of Cu<sup>2+</sup> peak, indicating partial reduction of Cu(OH)<sub>2</sub> to Cu during the CO<sub>2</sub>RR. After Ar etching (approximately 4 nm depth), as shown in Fig. S19b (ESI<sup>†</sup>), the disappearance of the Cu<sup>2+</sup> peak confirmed the presence of Cu(OH)<sub>2</sub> mainly at the surface (Fig. S19a, ESI<sup>†</sup>). The XPS peaks for post-reaction D\_Cu are in accordance with the pre-reaction state (Fig. S20a-b, ESI<sup>†</sup>), suggesting minimal changes in the catalyst.

To understand the promotional mechanism of the OH species on Cu for CO<sub>2</sub>RR, we calculated the CO<sub>2</sub>RR reaction path for C<sub>2</sub>H<sub>4</sub> on Cu(111) surface employing density functional theory (DFT). The potential energy surfaces with and without hydroxylation were compared, as shown in Fig. 3c. The corresponding structures of the intermediates were listed in Fig. S21 (ESI<sup>†</sup>). For the first CO<sub>2</sub> activation step, the intermediate \*COOH on the clean Cu surface has a relatively higher energy (0.46 eV), while an additional OH group brings its energy below zero. This result is consistent with the in situ Raman spectroscopy in Fig. 3a and 3b, where CO was observed much earlier (lower voltage needed) after hydroxylation. After hydroxylation, the energy of \*CO-CO coupling decreases from 0.43 eV to nearly 0 eV. This demonstrates a good agreement with the experimental observations that M\_Cu exhibited lower overpotential and higher Faradaic efficiency of ethylene compared to D\_Cu. Furthermore, the rate-determining step (\*CO-COH to \*CCO) for Cu-OH structure showed a lower energy barrier of 0.38 eV than that of bare Cu (0.58 eV), which is consistent with the low CO<sub>2</sub>RR overpotential of M\_Cu.

In summary, we present an efficient CO<sub>2</sub>RR electrode, where uniformly dispersed nano-sized copper particles were

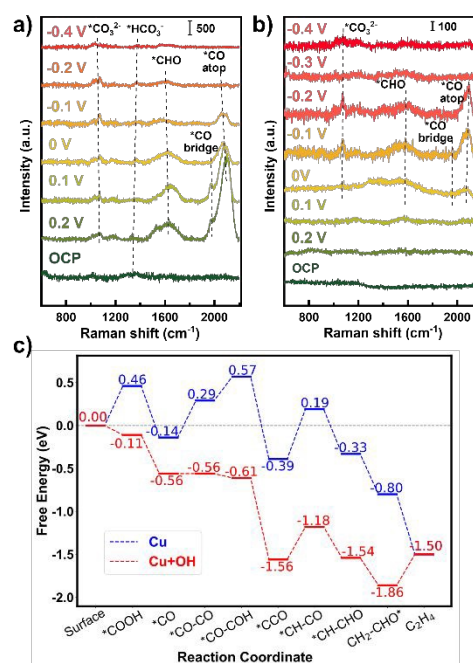


**Fig. 3** In situ Raman spectra of (a) M\_Cu; (b) D\_Cu. (c) DFT calculated free energy diagram of the CO<sub>2</sub>RR path for C<sub>2</sub>H<sub>4</sub> on Cu(111) surface with and without hydroxylation.



onto a PTFE substrate using ion sputtering. The hydrophobic PTFE effectively inhibited the H<sub>2</sub> evolution and enhanced the solid–liquid–gas interfaces. Particularly, the surface \*OH on the electrode was elegantly modulated by sputtering in a moist Ar atmosphere. The prepared M<sub>2</sub>Cu with increased surface \*OH coverage achieved a FE<sub>C<sub>2</sub>H<sub>4</sub></sub> over 50% at an exceptionally low potential of -246 mV, with an optimal ethylene Faradaic efficiency of 60.3%. Through in situ Raman spectroscopy and DFT calculations, it has been elucidated that the surface \*OH species facilitates both the activation of CO<sub>2</sub> and the C-C coupling steps. This work demonstrates a novel strategy for the modification of Cu-based catalysts for low-potential CO<sub>2</sub>RR to ethylene with high activity and selectivity. We believe our findings deepen the comprehension of CO<sub>2</sub> electroreduction mechanisms and contribute valuable insights for the efficient design of catalysts.

The manuscript was written through contributions of all authors. All authors have given approval to the final version of the manuscript.

This work was supported by the Strategic Priority Research Program of the Chinese Academy of Sciences (grant no. XDA0400000), the National Natural Science Foundation of China (grant no.22179141, and 22309199), the Youth Innovation Promotion Association Chinese Academy of Sciences (2023270), the Talent Plan of Shanghai Branch, Chinese Academy of Sciences (CASSHB-QNPD-2023-006), and the Photon Science Center for Carbon Neutrality.

## Conflicts of interest

There are no conflicts to declare.

## Data availability

The datasets supporting this article have been uploaded as part of the ESI.†

## Notes and references

- P. De Luna, C. Hahn, D. Higgins, S. A. Jaffer, T. F. Jaramillo and E. H. Sargent, *Science*, 2019, **364**, eaav3506.
- O. S. Bushuyev, P. De Luna, C. T. Dinh, L. Tao, G. Saur, J. van de Lagemaat, S. O. Kelley and E. H. Sargent, *Joule*, 2018, **2**, 825–832.
- Y. Y. Birdja, E. Pérez-Gallent, M. C. Figueiredo, A. J. Göttle, F. Calle-Vallejo and M. T. M. Koper, *Nat. Energy*, 2019, **4**, 732–745.
- C. Zhan, F. Dattila, C. Rettenmaier, A. Bergmann, S. Köhl, R. García-Muelas, N. López and B. R. Cuenya, *ACS Catal.*, 2021, **11**, 7694–7701.
- H. F. Li, T. F. Liu, P. F. Wei, L. Lin, D. F. Gao, G. X. Wang and X. H. Bao, *Angew. Chem. Int. Ed.*, 2021, **60**, 14329–14333.
- C. Choi, S. Kwon, T. Cheng, M. J. Xu, P. Tieu, C. Lee, J. Cai, H. M. Lee, X. Q. Pan, X. F. Duan, W. A. Goddard and Y. Huang, *Nat. Catal.*, 2020, **3**, 804–812.
- A. Bagger, W. Ju, A. S. Varela, P. Strasser and J. Rossmeisl, *Chemphyschem*, 2017, **18**, 3266–3273.
- K. Tran and Z. W. Ulissi, *Nat. Catal.*, 2018, **1**, 696–703.
- C. T. Dinh, T. Burdyny, M. G. Kibria, A. Seifitokaldani, C. M. Gabardo, F. P. G. de Arquer, A. Kiani, J. P. Edwards, P. De Luna, O. S. Bushuyev, C. Q. Zou, R. Quintero-Bermudez, Y. J. Pang, D. Sinton and E. H. Sargent, *Science*, 2018, **360**, 783–787.
- J. Huang, J. W. Dai, J. N. Zhu, R. Chen, X. Q. Fu, H. F. Liu and G. F. Li, *J. Catal.*, 2022, **415**, 134–141.
- J. Zhang, Z. P. Liu, H. S. Guo, H. R. Lin, H. Wang, X. Liang, H. L. Hu, Q. B. Xia, X. X. Zou and X. X. Huang, *ACS Appl. Mater. Interfaces*, 2022, **14**, 19388–19396.
- S. H. Chen, C. L. Ye, Z. W. Wang, P. Li, W. J. Jiang, Z. C. Zhuang, J. X. Zhu, X. B. Zheng, S. Zaman, H. H. Ou, L. Lv, L. Tan, Y. Q. Su, J. Ouyang and D. S. Wang, *Angew. Chem. Int. Ed.*, 2023, **62**.
- M. Dhiman, Y. Y. Chen, Y. F. Li, A. B. Laursen, K. U. D. Calvinho, T. G. Deutsch and G. C. Dismukes, *J. Mater. Chem. A*, 2023, **11**, 717–725.
- P. An, L. Wei, H. Li, B. Yang, K. Liu, J. Fu, H. Li, H. Liu, J. Hu, Y.-R. Lu, H. Pan, T.-S. Chan, N. Zhang and M. Liu, *J. Mater. Chem. A*, 2020, **8**, 15936–15941.
- S. Y. Lee, H. Jung, N.-K. Kim, H.-S. Oh, B. K. Min and Y. J. Hwang, *J. Am. Chem. Soc.*, 2018, **140**, 8681–8689.
- S. Mu, H. Lu, Q. Wu, L. Li, R. Zhao, C. Long and C. Cui, *Nat. Commun.*, 2022, **13**, 3694.
- G. Iijima, T. Inomata, H. Yamaguchi, M. Ito and H. Masuda, *ACS Catal.*, 2019, **9**, 6305–6319.
- M. X. Sun, A. Staykov and M. Yamauchi, *ACS Catal.*, 2022, **12**, 14856–14863.
- M. Li, T. Li, C. Sun, Y. Li, P. Wan, J. Qin, R. Gao, Y. Lv and Y. Song, *Mater. Today Energy*, 2024, **42**, 101568.
- T.-K. Cheng, N. Jeromiyas, Y.-K. Lin, C.-C. Yang, C.-L. Kao, P.-Y. Chen and C.-L. Lee, *Appl. Surf. Sci.*, 2024, **660**, 159978.
- Z. Xing, L. Hu, D. S. Ripatti, X. Hu and X. Feng, *Nat. Commun.*, 2021, **12**, 136.
- H. Liu, C. H. Yang, T. Bian, H. J. Yu, Y. M. Zhou and Y. W. Zhang, *Angew. Chem. Int. Ed.*, 2024, **63**, e202404123.
- X. B. Xu, D. F. Xiao, Y. G. Gao, W. B. Li, M. M. Gao, S. Zhao, Z. Y. Wang, Z. K. Zheng, P. Wang, H. F. Cheng, Y. Y. Liu, Y. Dai and B. B. Huang, *ACS Appl. Mater. Interfaces*, 2024, **16**, 16243–16252.
- B. M. Marsh, J. Zhou and E. Garand, *J. Phys. Chem. A*, 2014, **118**, 2063–2071.
- Z. X. Gu, H. Shen, Z. Chen, Y. Y. Yang, C. Yang, Y. L. Ji, Y. H. Wang, C. Zhu, J. L. Liu, J. Li, T. K. Sham, X. Xu and G. F. Zheng, *Joule*, 2021, **5**, 429–440.
- R. Z. Chen, L. Cheng, J. Z. Liu, Y. T. Wang, W. X. Ge, C. Q. Xiao, H. Jiang, Y. H. Li and C. Z. Li, *Small*, 2022, **18**.
- Y. B. Ma, J. L. Yu, M. Z. Sun, B. Chen, X. C. Zhou, C. L. Ye, Z. Q. Guan, W. H. Guo, G. Wang, S. Y. Lu, D. S. Xia, Y. H. Wang, Z. He, L. Zheng, Q. B. Yun, L. Q. Wang, J. W. Zhou, P. Y. Lu, J. W. Yin, Y. F. Zhao, Z. B. Luo, L. Zhai, L. W. Liao, Z. L. Zhu, R. Q. Ye, Y. Chen, Y. Lu, S. B. Xi, B. L. Huang, C. S. Lee and Z. X. Fan, *Adv Mater*, 2022, **34**.
- J. J. Shan, Y. X. Shi, H. Y. Li, Z. Y. Chen, C. Y. Sun, Y. Shuai and Z. J. Wang, *Chem Eng J*, 2022, **433**.
- M. Sun, A. Staykov and M. Yamauchi, *ACS Catalysis*, 2022, **12**, 14856–14863.
- Z. Y. Yin, J. Q. Yu, S. W. Yu, Z. H. Xie, L. Y. Zhang, T. Akauola, J. G. G. Chen, W. Y. Huang, L. Qi and S. Zhang, *Journal of the American Chemical Society*, 2022, **144**, 20931–20938.
- Y. Q. Zheng, J. W. Zhang, Z. S. Ma, G. G. Zhang, H. F. Zhang, X. W. Fu, Y. Y. Ma, F. Liu, M. C. Liu and H. W. Huang, *Small*, 2022, **18**.
- S. Hong, H. G. Abbas, K. Jang, K. K. Patra, B. Kim, B. U. Choi, H. Song, K. S. Lee, P. P. Choi, S. Ringe and J. Oh, *Adv Mater*, 2023, **35**.
- S. Wang, J. L. Zhang, L. Yao, Y. S. Yang, L. R. Zheng, B. Guan, Y. Z. Zhao, Y. Y. Wang, B. X. Han and X. Q. Xing, *Nano Res*, 2023, **16**, 10779–10786.
- L. J. Zhu, D. H. Si, F. X. Ma, M. J. Sun, T. Zhang and R. Cao, *ACS Catalysis*, 2023, **13**, 5114–5121.



## Data availability

The data supporting this article have been included as part of the ESI.†

